
Sensitivity of Stratospheric Retrievals from Radio Occultations on Upper Boundary Conditions

Chi O. Ao¹, George A. Hajj¹, Byron A. Iijima¹, Anthony J. Mannucci¹, Thomas M. Schröder¹, Manuel de la Torre Juárez¹, and Stephen S. Leroy²

¹ Jet Propulsion Laboratory, California Institute of Technology, Pasadena, USA
chi.o.ao@jpl.nasa.gov

² Department of Chemistry and Chemical Biology, Harvard University, Cambridge, USA

Summary. The main uncertainty in the stratospheric retrievals from GPS radio occultation (RO) measurements comes from the lack of reliable measurements in the upper stratosphere and above where the bending due to the neutral atmosphere is weak and residual ionospheric effects are strong. In this work, we quantify the bias and uncertainty of the refractivity and temperature retrievals due to different upper boundary strategies using a simulation study. We use lidar refractivity and temperature profiles as the input states in generating the synthetic occultations. Random noise levels commensurate with the CHAMP RO measurements are then added to the simulated data. Through this study, the sensitivity of stratospheric retrievals to upper boundary methods and parameters are examined. Such error characterizations are important prerequisites towards the effective use of GPS RO data in climate monitoring.

1 Introduction

GPS radio occultation (RO) has been touted as one of the most promising remote sensing techniques in climate monitoring because RO measurements are self-calibrating and are not subject to time-dependent biases due to instrumental drifts. Over the years, the precision, accuracy, and resolution of the measurements, especially in the altitude range of 5–25 km, has been well-established through theoretical considerations (e.g., [1]), validation studies (e.g., [2]), and inter-satellite comparison [3]. However, stratospheric retrievals at altitudes higher than 25 km are more uncertain. This is mainly due to the lack of reliable measurements in the upper stratosphere and above where the bending due to the neutral atmosphere is weak compared with various error sources including thermal noise, orbital and local multipath errors, and perhaps most significantly, uncorrected ionospheric effects [1]. A solution for

this problem is to replace the noisy bending angles at high altitudes (typically above 40–60 km) with “modeled” bending angles obtained from a climatology such as MSIS [4]. The influence of the modeled bending angles decreases as the altitude decreases. The possible problem with this approach is that the retrievals could become biased towards the adopted climatology. An alternative, climatology-independent approach is to extrapolate the data at lower altitudes upward to altitudes where the data are not trustworthy. The problem with the extrapolation approach is that it relies on questionable assumptions regarding the characteristics of the stratosphere and mesosphere.

While there has been numerous published works addressing the upper boundary treatments and the retrieval errors associated with them [1, 5, 6, 7, 8, 9], the present study is unique in that the retrieval errors are examined with a simulation study which is based on atmospheric profiles from lidar measurements. The lidar profiles are more representative of the real stratospheric and mesospheric conditions than available models (albeit much more localized spatially and temporally) and are relatively independent of climatology. Thus they can be used to assess more quantitatively the errors due to the use of climatology as upper boundary conditions. The focus of this paper is to evaluate and compare the sensitivity of RO retrievals to the extrapolation and climatology approaches. We consider random bending angle noise at levels that are representative of CHAMP measurements.

The rest of the paper proceeds as follows. In Sec. 2, we give more details on the data and methodology used in this study. The numerical results are presented in Sec. 3, where we show refractivity and temperature errors under different upper boundary conditions. Finally, we summarize the main findings in Sec. 4 and discuss future work.

2 Data and Methodology

The input atmosphere used in the simulations is based on one year of lidar observations from Mauna Loa, Hawaii (19.5°N, 155.6°W) [10]. The retrieved lidar profiles are freely accessible from the Network for the Detection of Stratospheric Change (NDSC) web site (<http://www.ndsc.ncep.noaa.gov>). In the year 2001, a total of 156 profiles covering the altitude range 20–90 km are available. Since the contribution of water vapor to refractivity is negligible in the stratosphere and above, the refractivity profile can be derived simply from the lidar temperature and pressure profiles with the standard expression $N = 77.6(P/T)$, where P is the pressure in mbar and T is the temperature in Kelvin.

From the refractivity profile, and assuming local spherical symmetry, the bending angle can be obtained with the forward Abel integral (e.g., [1])

$$\alpha(a) = -2a \int_a^\infty \frac{da'}{\sqrt{a'^2 - a^2}} \frac{d \ln n}{da'} \quad (1)$$

where $a = n(r)r$ is the impact parameter and $n(r) = 1 + N(r) \times 10^{-6}$ is the index of refraction. Since input profiles only reach altitudes of ≈ 90 km, we extend the refractivity profiles beyond the maximum lidar altitude with exponential extrapolation. Because the atmosphere is so tenuous at these altitudes, the results presented here are not sensitive to the manner in which these profiles are extended there.

The next step is to add realistic level of noise to the simulated bending angles.

$$\alpha_{obs}(a) = \alpha(a) + \alpha_n(a) \quad (2)$$

Note that we have ignored the ionosphere in the computation of $\alpha(a)$. Thus we regard $\alpha_{obs}(a)$ as the ionosphere-free bending angle. Any residual calibration and ionosphere errors should be modeled in $\alpha_n(a)$. The choice of $\alpha_n(a)$ will be discussed more below.

In the presence of noise, $\alpha_{obs}(a)$ can be trusted only below certain ray height ($h = a - R$, where R is the local radius of curvature of the Earth), where the bending signal is large compared to the noise level. However, to obtain the refractivity at a lower ray height, we require bending angles at all ray heights above it. Thus, $\alpha_{obs}(a)$ above h needs to be replaced with external data or *a priori* model, $\alpha_{mod}(a)$. The refractivity profile is obtained from the Abel inversion integral as

$$\ln n(a) = \frac{1}{\pi} \int_a^{h+R} da' \frac{\alpha_{obs}(a')}{\sqrt{a'^2 - a^2}} + \frac{1}{\pi} \int_{h+R}^{\infty} da' \frac{\alpha_{mod}(a')}{\sqrt{a'^2 - a^2}} \quad (3)$$

The specification of $\alpha_{mod}(a)$ above h used (including the choice of h) will henceforth be referred to as the Abel boundary condition (ABC). As discussed in Sec. 1, current approaches to ABC can be grouped into two categories: *extrapolation* (EXT) and *climatology* (CLI).

In the EXT approach, the bending angle in the region below h is used to extrapolate the data to higher altitudes. No other external information is needed other than the functional form assumed in the extrapolation. We use a simple exponential function $\exp(b_0 + b_1 a)$ to characterize the bending angle above h with the parameters b_0, b_1 determined from fitting the data from $\approx (h - 10$ km) to h . The exponential functional form approximates an isothermal atmosphere. In the CLI approach, the observed bending angle in the region above h is replaced with bending derived from a climatology such as MSIS. Thus the replacement is completely independent of the observed bending angle and is not susceptible to noise in the data. The ideal ABC should be able to minimize the propagation of noise in the retrieved refractivity to lower altitudes while producing little or no bias.

Note from Eq. (3) that we have used a “hard” boundary where the $\alpha(a)$ switches from $\alpha_{obs}(a)$ to $\alpha_{mod}(a)$ at a fixed ray height h . An alternative approach is to adopt the so-called statistical optimization method where the measured and modeled bending angles are linearly combined to minimize the root-mean-square (rms) error in the bending angles (see [9] and references

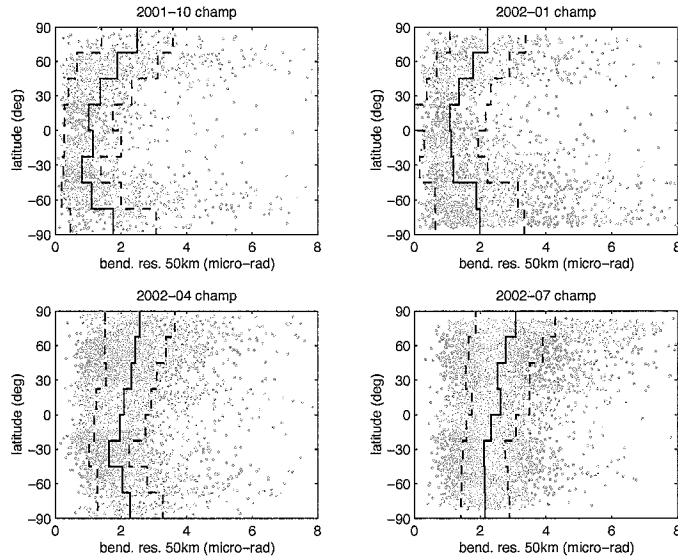


Fig. 1. Residuals of the ionosphere-corrected bending angle from four months of CHAMP data. Solid line indicates the median values within 20° latitudinal bands while dashed lines indicate the mean absolute deviation values about the median.

therein). The effective application of optimization method requires reasonable estimates of the variance and covariance characteristics of the measurements and model, which is a non-trivial task. The hard boundary is applied here because the results are much simpler to interpret.

A key ingredient in the simulation study is to come up with a realistic representation of the bending angle noise $\alpha_n(a)$. This, however, proves difficult because of the multitude of random and systematic error sources that might contribute to the ionosphere-free bending angle [1]. For simplicity, we assume that the noise is characterized by a random Gaussian process with standard deviation which is independent of altitude. The level of random noise can be determined through the examination of CHAMP bending angles. Fig. 1 shows the rms residual of the ionosphere-free bending angle obtained by linearly detrending $\alpha_{obs}(a)$ with ray heights between 50 to 55 km. Interesting seasonal and latitudinal variations can be noted, with significantly more scatters in the polar regions. From the figure, it can be concluded that bending angle residuals for most of the CHAMP occultations fall between 1 to 4 μrad . For comparison, the U.S. Standard atmosphere gives a bending angle of about 5 μrad at 60 km and 8 μrad at 45 km. To obtain a reasonable upper bound on the averaged errors, we consider in the following bending angle noise with 4 μrad standard deviation and examine the retrieved refractivity and temperature profiles resulting from ABC strategies with upper boundary heights from 45 to 60 km.

3 Simulation results

3.1 Refractivity errors

Consider first the noiseless case. Fig. 2 shows the mean and rms fractional refractivity errors corresponding to different ABC strategies (EXT and CLI approaches, with upper boundary heights $h = 45, 50, 55, 60$ km). These results are obtained by averaging the errors over the 156 simulated occultations. In the noiseless case, the refractivity errors are entirely due to the inaccurate modeling of the atmosphere above h . As expected, the mean and rms errors increase as h decreases. The bias is positive for the CLI approach and mostly negative for the EXT approach.

Fig. 3 shows the corresponding results for the case with $4 \mu\text{rad}$ bending angle noise. While the mean errors remain at about the same level as the noiseless case, the rms errors are now several times larger. It should be noted that lowering the upper boundary height h has relatively little impact on reducing the rms errors, indicating that the rms errors are dominated by the bending angles below 45 km ray heights.

These results show that for both EXT and CLI approaches, it is far better to use an upper boundary height which is in the range of 55–60 km. These strategies yield the smallest biases without introducing significantly larger rms errors. For the $4 \mu\text{rad}$ noise case, $h = 55$ km gives a refractivity bias of -0.05%

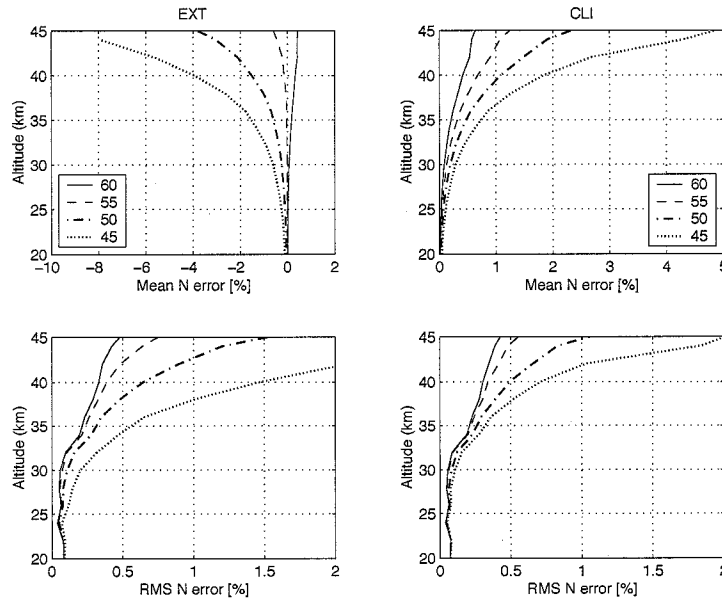


Fig. 2. Fractional refractivity errors for EXT and CLI strategies with upper boundary heights at 45, 50, 55, 60 km: noiseless case.

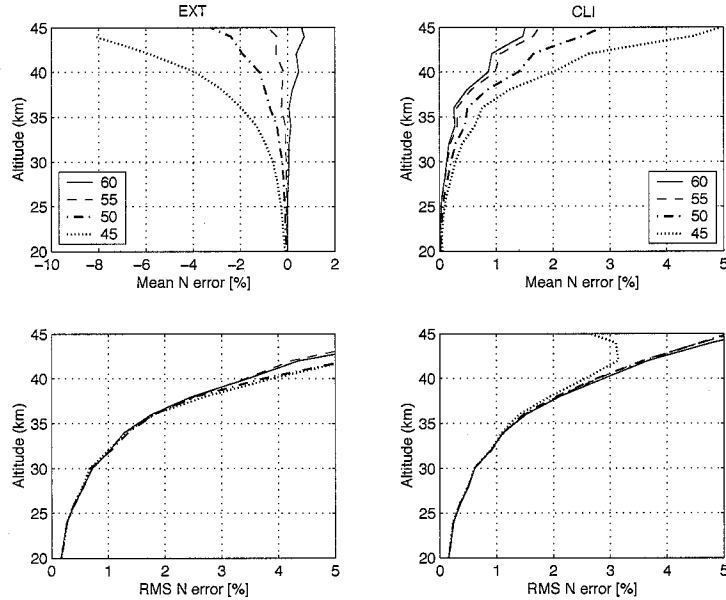


Fig. 3. Fractional refractivity errors for EXT and CLI strategies with upper boundary heights at 45, 50, 55, 60 km: $4 \mu\text{rad}$ case.

and rms error of 0.71% at $z = 30$ km for EXT. For CLI, the corresponding refractivity bias is 0.14% with rms error of 0.61%. Thus EXT and CLI results are quite comparable, with CLI yielding a smaller rms error at the cost of a larger bias.

3.2 Temperature errors

To derive the temperature profile from refractivity profile [1], we initialize the hydrostatic equation with the input temperature at 40 km. Figs. 4 and 5 show the temperature errors for the noiseless case and the case with $4 \mu\text{rad}$ bending angle noise respectively for different ABC approaches. Because the temperature is fixed at the initialization height of 40 km, the maximum temperature errors occur at altitudes slightly below 40 km. At 30 km, the mean temperature error for the $4 \mu\text{rad}$ noise with $h = 55$ km case is -0.50 ± 2.71 K for EXT and 0.40 ± 2.35 K. The rms errors become less than 1 K below 20 km for all ABC strategies.

When retrieving real data, we do not have the luxury of knowing the actual temperature. Errors in the initialization temperature introduce additional errors in the retrieved temperature profiles, although such errors decrease rapidly away from the initialization height. This is illustrated in Fig. 6, which shows the mean and rms temperature errors when the initialization temperature error is varied from 0 to 10 K for the EXT strategy with $h = 55$ km.

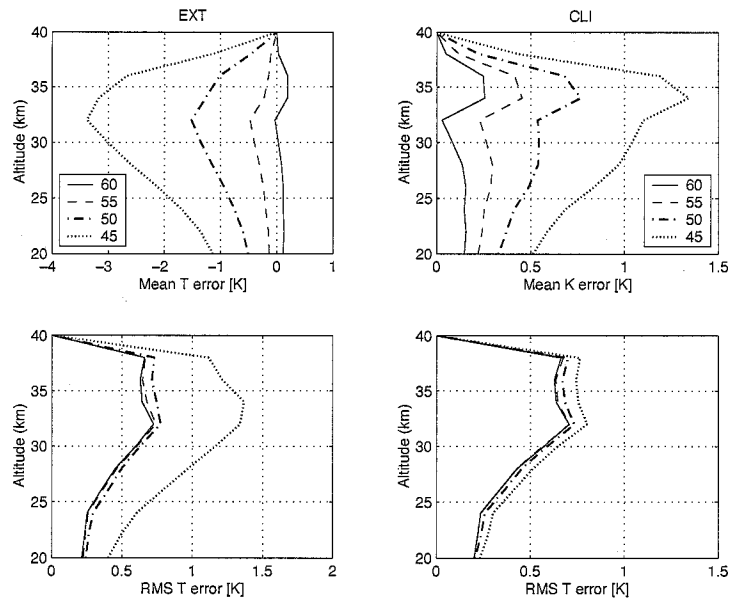


Fig. 4. Temperature errors for EXT and CLI strategies with upper boundary heights at 45, 50, 55, 60 km: noiseless case.

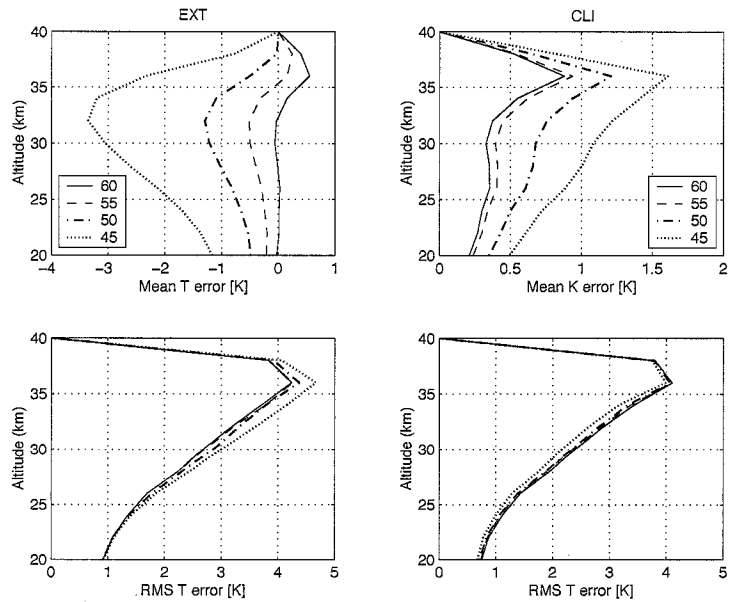


Fig. 5. Temperature errors for EXT and CLI strategies with upper boundary heights at 45, 50, 55, 60 km: $4 \mu\text{rad}$ case.

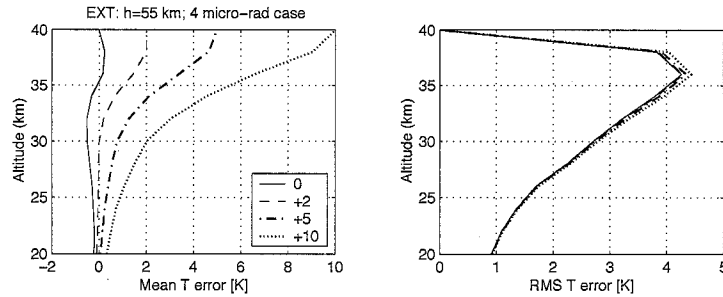


Fig. 6. Temperature errors due to temperature initialization error based on EXT approach with $h = 55$ km and $4 \mu\text{rad}$ bending angle noise.

In the worst case with 10 K initialization error, the mean temperature error becomes 2.04 K at 30 km, but it drops to only 0.36 K at 20 km.

4 Conclusion

The simulation results presented here suggest that EXT and CLI upper boundary conditions yield comparable levels of biases and rms errors in refractivity and temperature below 40 km when upper boundary heights at ≈ 55 –60 km are used. Lower h (especially $h = 45$ km for EXT) leads to much larger biases without a significant benefit in reducing the rms errors. For the higher upper boundary heights, a bias on the order of 0.5 K can be expected at 30 km if the initialization temperature is exact. This bias increases to about 2 K if we assume a 10 K temperature initialization error. The simulation results also confirm the sub-Kelvin accuracy of temperature retrievals below 20 km, achieved under fairly noisy conditions and with great insensitivity to the Abel upper boundary conditions and temperature initialization.

The present study is rather limited in scope in that it only considers the atmospheric conditions in one tropical location. A more robust evaluation requires extending the study to multiple locations around the globe. In addition, only the gross statistical characteristics of the retrieval errors have been examined thus far. The key question on the influence of climatology in deducing interannual variability or long-term climate trends has not been specifically addressed. We believe that further simulation studies of the kind performed here can be instrumental in clarifying such issues.

Acknowledgment

This research was carried out at the Jet Propulsion Laboratory, California Institute of Technology, under a contract with the National Aeronautics and Space Administration.

References

1. E. R. Kursinski, G. A. Hajj, J. T. Schofield, R. P. Linfield, and K. R. Hardy. Observing Earth's atmosphere with radio occultation measurements using the Global Positioning System. *J. Geophys. Res.*, 102(D19), 23429–23465, 1997.
2. C. Rocken, R. Anthes, M. Exner, D. Hunt, S. Sokolovskiy, R. Ware, M. Gorbunov, W. Schreiner, D. Feng, B. Herman, Y.-H. Kuo, and X. Zou. Analysis and validation of GPS/MET data in the neutral atmosphere. *J. Geophys. Res.*, 102(D25), 29849–29866, 1997.
3. G. A. Hajj, C. O. Ao, B. A. Iijima, D. Kuang, E. R. Kursinski, A. J. Mannucci, T. K. Meehan, L. J. Romans, M. de la Torre Juárez, and T. P. Yunck. CHAMP and SAC-C atmospheric occultation results and intercomparisons. *J. Geophys. Res.*, 109, D06109, doi:10.1029/2003JD003909, 2004.
4. J. M. Picone, A. E. Hedin, D. P. Drob, and A. C. Aikin. NRLMSISE-00 empirical model of the atmosphere: Statistical comparisons and scientific issues. *J. Geophys. Res.*, 107(A12), 1468, 2002.
5. K. Hocke. Inversion of GPS meteorology data. *Ann. Geophys.*, 15:443–450, 1997.
6. A. K. Steiner, G. Kirchengast, and H. P. Ladreiter. Inversion, error analysis, and validation of GPS/MET occultation data. *Ann. Geophys.*, 17, 122–138, 1999.
7. S. B. Healy. Smoothing radio occultation bending angles above 40 km. *Ann. Geophys.*, 19, 459–468, 2001.
8. M. J. Rieder and G. Kirchengast. Error analysis and characterization of atmospheric profiles retrieved from GNSS occultation data. *J. Geophys. Res.*, 106(D23), 31755–31770, 2001.
9. M. E. Gorbunov. Ionospheric correction and statistical optimization of radio occultation data. *Radio Sci.*, 37(5), 1084, doi:10.1029/2000RS002370, 2002.
10. T. Leblanc and I. S. McDermid. Quasi-biennial oscillation signatures in ozone and temperature observed by lidar at Mauna Loa, Hawaii (19.5°N, 155.6°W). *J. Geophys. Res.*, 106(D14), 14869–14874, 2001.